Study on solid electrolyte catalyst poisoning in solid acid fuel cells

Maximilian Wagner[a†], Oliver Lorenz[a], Felix P. Lohmann-Richters[b], Aron Varga[c] and Bernd Abel[a]

[a]Leibniz Institute for Surface Engineering, Department of Functional Surfaces, Permoserstraße 15, 04318 Leipzig, Germany

[b]Forschungszentrum Jülich GmbH, Institut für Energie- und Klimaforschung - Elektrochemische Verfahrenstechnik (IEK-14), 52425 Jülich, Germany

[c]BMW Group, Department Electrical Drive Development, Taunusstraße 41, 80807 Munich, Germany

†maximilian.wagner@iom-leipzig.de, Tel.: +49 341 235 3365, Fax.: +49 341 235 2584

Keywords: solid acid fuel cell; intermediate temperature fuel cells; cyclic voltammetry; impedance spectroscopy; phosphate poisoning

Abstract

Solid acid fuel cells operate at intermediate temperatures utilizing a solid electrolyte (CsH_2PO_4, CDP). However, relatively little is known about the degradation mechanism and the topic is rarely addressed. Phosphate poisoning of the platinum catalyst is a well-known problem for fuel cells working with H_3PO_4 as electrolyte. With CsH_2PO_4 as electrolyte, phosphate poisoning is therefore likely to occur as well. In this study we show a fast and reversible degradation behavior of solid acid fuel cells and associate it with poisoning of the catalyst. After a decline in power output of around 50% within hours, an in situ reactivation of the cell to almost the initial performance was possible by multiple cycling between the voltage of 0.1 V and 2.0 V. A limitation of the effect to the cathode is shown and the underlying process was analyzed by changes in the low frequency domain of impedance measurements, which is indicating a catalyst poisoning, and by the dependency from the upper vertex voltage. By employing a micro porous current collector, a decrease in the low frequency domain as well as enhanced stability (<125 $\mu V\ h^{-1}$ at 0.43 V) was achieved. This work extends from a detailed insight in the degradation

mechanism of solid acid fuel cells, to providing a working electrode modification to prevent poisoning, establishing a promising electrode stability on a laboratory scale.

1 Introduction

Intermediate temperature fuel cells are promising conversion devices and received a growing interest in the past years. Important representatives are the well investigated high temperature proton-exchange membrane fuel cells (HT-PEMFC) with an operating temperature range between 120 °C and 200 °C[1] and solid acid fuel cells (SAFC) operating between 228 °C and 260 °C.[2] The intermediate operating temperate allows good catalytic activity and fuel flexibility while relatively cheap structural elements can be used. The main difference between these fuel cell types is the type of electrolyte. While HT-PEMFC are based on membranes of polybenzimidazole (PBI) and/or pyridine polymers doped with concentrated and highly corrosive H_3PO_4, SAFC utilize CsH_2PO_4 as solid, non-toxic proton conducting electrolyte.[3–5] With a reversible phase transition at 228 °C, CsH_2PO_4 transforms from a paraelectric phase into proton conducting phase, increasing the proton conductivity by several orders of magnitude to about $2.2 \cdot 10^{-2}$ S cm^{-1}.[2,6,7] In the proton conducting phase, a reversible dehydration process from CsH_2PO_4 to cesium hydrogen pyrophosphate ($CsH_2P_2O_7$) and eventually to $CsPO_3$ occurs.[8] By hydrating the gas atmosphere, the onset temperature of the process can be greatly increased depending on the humidification level. Above temperatures of 260 °C however, a liquid transient phase ($CsH_{2(1-x)}PO_{4-x}$) was observed within a humidified atmosphere.[9] Papandrew et al. [10] and Wagner et al.[11] related this liquid phase to observed morphological changes occurring during operation. While doped PBI membranes achieve higher proton conductivities between $5 \cdot 10^{-2}$ S cm^{-1} and $7 \cdot 10^{-2}$ S cm^{-1} the operating temperature is limited by the thermal stability of phosphoric acid.[12]

Platinum is the most common choice as the catalyst for both SAFC and HT-PEMFC due to its high activity and stability.[1,13,14] During operation, hydrogen is oxidized at the anode. The generated protons are transported through the proton conducting electrolyte and form water during the rate limiting oxygen reduction reaction at the cathode. The reaction occurs at the so-called triple phase boundary, where the catalyst is in contact with the proton conducting electrolyte, the current collector and the

gas phase. The exact mechanism is still unclear, but recent work indicates a four electron reaction path as most likely for the oxygen reduction reaction (ORR).[15] To maximize the active site density especially at the cathode, high performance electrodes consist of platinum nanoparticle on carbon support well mixed with the electrolyte.[16] In case of HT-PEMFC, a binder to control the wettability of the gas diffusion layer is added.[1] While an optimization of the catalyst activity is desirable to reduce production costs, the stability of the catalyst and hence the lifetime of the fuel cell is currently the most important issue to achieve necessary industrial lifetimes of 40,000 h.[17] In solid acid fuel cells, the problem is rarely addressed. A densification of the porous cathode was reported in several cases.[10,11,18,19] In a previous study Wagner et al. discussed a correlation between local heating and morphological changes of the CsH_2PO_4.[11] Hotspots, localized around the current collector fibers were found be the origin of the morphological changes.[11] While model electrodes with a inhomogeneous current distribution showed a fast degradation, the stability was increased significantly by improving the current distribution or reducing the overall current density.[11] CsH_2PO_4 is known to react with numerous metals and metal oxides like Ru or Mo, forming nonconducting phases and can potentially poison platinum.[20] For HT-PEMFC, the adsorption of phosphate to platinum catalyst of the cathode in form of $H_2PO_4^-$ as well as the dissolution of the platinum are problematic and well investigated reactions. Comprehensive reviews on this topic are given by Prokop et al. and Zeis et al.[21,22] In general, phosphate adsorption to the catalyst is depending on the temperature and cell voltage and is most pronounced at the cathode. [23,24] The adsorbate is blocking active sites and causing dissolution of platinum nano particles by forming a platinum- phosphate complex.[25,26] For low temperature proton-exchange membrane fuel cells (LT-PEMFC), the poisoning was investigated thoroughly in half cells by cyclic voltammetry,[27] Fourier transformed infrared spectroscopy measurements (FTIR), [28,29] and X-ray absorption spectroscopy (XAS).[30,31] Phosphate groups adsorb strongly to the platinum surface and result in a decreasing ORR activity by blocking active sites. The degree of the coverage and geometry of the adsorbate is thereby dependent on the voltage, temperature, crystal face, and concentration.[31,32] These experiments were carried out at room temperature under laboratory conditions on a 111-platinum surface. However,

due to the higher operational temperature of the HT-PEMFC, the reactions and voltage values reported at a temperature of 25 °C may not be directly relevant to high temperature applications.[25] At the operating temperature of HT-PEMFC, H_3PO_4 is extremely corrosive to metals and their oxides.[33,34] It adsorbs strongly to the Pt surface of the cathode in the form of $H_2PO_4^-$, causing catalyst poisoning and formation of soluble metal-phosphate complexes.[21,22] At the anode, a small, voltage-independent phosphate adsorption causes only a negligible increase in the overvoltage of the hydrogen oxidation reaction (HOR).[35] By applying a Δμ technique to the X-ray near edge structure (Δμ- XANES) obtained during X-ray adsorption spectroscopy, Kaserer et al. were able to measure the adsorbates on a platinum surface in operando.[24] A voltage dependent adsorption was reported: Below 300 mV, hydrogen generated by the ORR and from the acidic environment is adsorbed on the surface. Between 300 mV and 800 mV phosphate groups are present with a co-adsorption of oxygen species. Above 800 mV oxygen adsorbates gradually forcing phosphate groups to leave the surface. Other published results merely differ in regard of the intensity and voltage range of the adsorption, but report the same tendency.[30,36,37] For example, high temperatures and voltages favor a single coordinated C_S geometry of the phosphate adsorbate, where a minimal space is needed on the platinum surface.[24,29,30] The high mobility of the C_s-adsorbates interferes with the Δμ-XANES technique. Thus, even at temperatures of 180 °C phosphate anions might be adsorbed to the catalyst surface and continuously blocking the ORR. Kaserer et al. concluded that higher operating temperatures are needed to completely clean the cathode from phosphate anions.[24] It is unclear if a temperature of ca. 240 °C, the operating conditions of SAFCs, may change this adsorption process.

The reduction and oxidation kinetics of adsorbed PO_4 anions has been investigated in literature and different phosphorous reduction products were identified. These phosphorous species tend to adsorb strongly to the catalyst resulting in severe poisoning.[38,39] At low voltages, hydrogen atoms are adsorbed at the surface of the cathode due to the water produced from the ORR and the phosphoric acid electrolyte. Doh et al. proposed a chemical rather than electrochemical reduction pathway.[40] Kaserer et al. [24] reported hydrogen adsorption at the cathode below a voltage of 300 mV vs a pseudo reference

electrode, while Prokop et al.[26] discussed a reduction onset at 0.43 V vs dynamic hydrogen electrode (DHE). The nature of the reduction products was studied in detail and H_3PO_3, H_3PO_2 and elemental phosphorus have been reported to be present at the catalyst surface.[26,38–43] The reduced compounds remain adsorbed on the Pt surface blocking the active sites for the ORR. In the voltage region of platinum oxidation these phosphorous species get oxidized to PO_4-species again.[41,42,44] Platinum dissolution is another phosphate associated degradation process. In general, it takes place at voltages close to open circuit conditions and is pronounced only for nano particles but not for bulk material. It is mainly caused by the chemical dissolution of PtO_x to Pt^{2+}_{sol} on smaller Pt nanoparticles, followed by a subsequent redeposition of Pt^{2+}_{sol} on larger particles. The electrochemical oxidation to PtO_x was determined as rate limiting step of this reaction.[26] While different scientific studies focusing on Pt dissolution for H_3PO_4 based electrolytes at elevated temperatures exist, a similar behavior caused by CsH_2PO_4 has not been studied comprehensively.[23,25,26] Work of Lohmann-Richters et al. indicate that degradation routes are different in SAFC with platinum dissolution and particle growth are slower, as there is no liquid phase available.[45] Lohmann-Richters further suspected different degradation processes for SAFC electrodes including phosphate poisoning.[46] Compared to phosphoric acid, CsH_2PO_4 is a less corrosive, solid state electrolyte where the phosphate anions are fixed to their places in the crystal structure. In case of a liquid transition state however, a similar poison reaction could occur at the platinum surface. Ghoshal et al. studied the phosphate adsorption to platinum and chalcogenides and demonstrated a RuMoSe/C based SAFC electrode with a high phosphate tolerance and remarkable stability over 120 h.[20]

In this work, we show that platinum poisoning by phosphate adsorption and subsequent reduction can occur in SAFC despite the operating temperature of ca. 240 °C and the solid-state electrolyte. The poisoning effects are investigated by constant current and cyclic voltammetry measurements, scanning electron microscopy imaging as well as impedance spectroscopy. Cyclic generation and reduction of PtO_x leads to a transient reactivation of the electrode performance. Increasing the electric contact of the catalyst by employing a micro porous current collector significantly improved the

stability. These results enable a better understanding of platinum stabilization and degradation of SAFC electrodes and represent a big step towards long term stable high-performance electrodes.

2 Experimental section

2.1 Electrolyte synthesis and membrane electrode assembly fabrication

The synthesis of the electrolyte CsH_2PO_4 was described in detail previously.[47] In a nutshell, H_3PO_4 (85 %, Carl Roth) was mixed with methanol (99.9 %, anhydrous, Alfa Aesar) and a stoichiometric equivalent of Cs_2CO_3 (99%, Alfa Aesar), dissolved in methanol was added to the mixture. The suspension was filtrated, washed and dried over night at 80 °C. The resulting CsH_2PO_4 powder was pressed (GS25440-AtlasTM Automatic 15T) at 250 MPa for five minutes into dense polycrystalline electrolyte pellet (20 mm in diameter, 1 mm in thickness). Different electrodes were applied to the electrolyte pellet and the resulting membrane electrode assembly (MEA) sandwiched between carbon paper (CP) acting as electron collectors and gas diffusion layers (PACOPOR ST 60 AL3, PACO Paul GmbH und Co. KG) before electrochemical characterization, see Table 1. Platinum thin film electrodes were applied using DC magnetron sputtering (Edwards Auto 306, 300W, 5 mTorr Ar). The deposition of a 60 nm thick platinum layer was controlled by a quartz crystal micro balance and resulted in 128 $\mu g_{Pt}\ cm^{-2}$ platinum per electrode. A small diffusion limitation of hydrogen through the platinum thin film is reported for the anode side at this thickness.[48] Platinum thin films have been shown as a functional electrodes for the ORR and increasing the area increased the activity of the anode and cathode on a similar scale.[49,50] Three different types of MEAs were fabricated for this work. An overview is given in Table 1.

Table 1 Overview of characterization and fabrication details for all relevant MEAs.

MEA-Type	Electrochemical characterization	Electron collector	Cell symmetry	Electrode type
CP/Pt@CDP	CC, OCV, CV, IVC, SPEIS	CP[a]	symmetric	Sputter deposited Pt thin film on CsH_2PO_4 pellet

Pt@CP_{MPL}/CDP	CC, OCV, CV, ICV, SPEIS	CP_{MPL}[b]	symmetric	Sputter deposited Pt thin film on CP_{MPL}
Pt/CDP/powder	CC, OCV, CV	CP[a]	asymmetric	(1) Sputter deposited Pt thin film (2) powder containing CsH_2PO_4, Pt and Pt on carbon[c]

[a]Carbon paper: Toray Inc. TGP-60. [b]Carbon paper: Toray Inc. TGP-H-60-MPL. [c]mixed electrode containing CsH_2PO_4, Pt-black (99.9%, fuel cell grade, Aldrich) and Pt on carbon (40%, HiSPEC4100, Alfa Aesar) in a 3:3:1 mass ratio.[51] CC: constant current, OCV: open circuit voltage, CV: cyclic voltammetry, IVC: I-V characterization, SPEIS: staircase potential electrochemical impedance spectroscopy.

The first MEA, denoted as CP/Pt@CDP, has a symmetric design with a platinum thin film applied on the CsH_2PO_4 pellet on both sides. This electrode design was introduced by Louie et al. in 2011[48] and is used in this work as a model electrode to show a degradation on a reasonable time scale. Previous studies have shown that the carbon fibers are in contact with only 20 % of the platinum surface, resulting in inhomogeneous current distribution and hot spot formation.[11] For Pt@CP_{MPL}/CDP MEAs, the pressed electrolyte pellet was sandwiched by carbon paper with a micro porous layer (Toray Inc. TGP-H-60-MPL) on one side, at which a platinum thin film was sputtered on previously. Pt/CDP/powder MEAs have a asymmetric design with one electrode consisting of a platinum thin film and the other of a powder electrode, similar to the one reported by Uda et al.[51]. Symmetric powder/CDP/powder MEA have the same powder electrode as anode and cathode. For the fabrication of a powder electrode, CsH_2PO_4 (grinded), Pt-black (99.9%, Aldrich) and Pt on carbon (40%, HiSPEC4100, Alfa Aesar) were mixed in a 3:3:1 mass ratio with a resulting platinum loading of 7.7 mg cm^{-2}. The electrode powder mixture was evenly distributed on the pressed electrolyte pellet and compacted at 125 MPa for five minutes.

2.2 Characterization

Scanning electron microscopy (SEM, Ultra 55 SEM, Carl Zeiss Ltd.) images were recorded using an secondary electron (SE) detector with an acceleration voltage of 5 keV. Identification of the different phases visible on the electrode surface was performed using a back-scattered electron (BSE) detector with an accelerated voltage of 2 keV and energy-dispersive X-ray spectroscopy (ZEISS 1550VP Field Emission SEM, Bruker EDX XFlash 3001) with an acceleration voltage of 8 keV. The respective images are given in the supplementary information (ESI, S1). X-ray photoelectron spectroscopy (XPS) of a CP/Pt@CDP MEA was carried out on a X-ray photoelectron spectrometer (Kratos, Axis Ultra) with monochromatic Al-K_α radiation. The anode and cathode were investigated after operating for 15 h at a constant current of 10 mA cm^{-2}. Separation of the catalyst layer from the electrolyte was done by multiple washing cycles. For each washing cycle, the platinum layer was submerged in 100 ml of water for 10 min. After five cycles, no phosphate could be detected by ion chromatography. For electrochemical characterization, the complete cells were placed in a custom-made cell holder and heated to 240 °C. Humidification was achieved by passing the gas flow through 80 °C water at a flowrate of 75 sccm. The resulting water partial pressure of 0.4 atm was well within the region of safe operation.[18] The respective partial pressure of hydrogen and oxygen during operation was 0.6 atm, yielding a total pressure of 1 atm at both electrodes. The gas feed at a flowrate of 75 sccm is orders of magnitude higher than the electrochemical reactant consumption or water generation. Electrochemical data was recorded with a Biologic VSP 300 potentiostat, with the cathode serving as working electrode and the anode as both counter and pseudo-reference electrode in all cases. Such a configuration has been used in other studies already.[45,52–54] Constant current (CC) measurements were done at current density of 10 mA cm^{-2} and the open circuit voltage (OCV) was determined after each CC measurement. Occasional fluctuations in the gas flow rate (once or twice every 20 h) caused short, reversible fluctuations of the cell voltage during long term measurements. To avoid confusion, these fluctuations were removed from the measurements in the manuscript. The averaged measured open circuit voltage was 0.90 V ± 0.03 V and showed no significant time dependency (ESI, S2). Staircase

potential electrochemical impedance spectroscopy (SPEIS) with a 10 mV perturbation amplitude over a frequency range of 10 kHz to 100 mHz was recorded at voltages of 0.05 V and 0.35 V. To estimate the nominal zero frequency impedance, I-V characterization (IVC) from OCV to 0 V with a scan speed of 10 mV s^{-1} was done before each SPEIS measurement and the slope obtained from fitting at the respective voltages. The coefficient of regression (R^2) of linear regression around the respective voltages was above 0.9997 in all cases. A cyclic voltammetry (CV) measurement consisted of a series of 16 cycles each cycling with a scan rate of 50 mV s^{-1}. In a separate experiment, CV scan rates of 150 mV s^{-1}, 50 mV s^{-1} and 15 mV s^{-1} were investigated, and the results given in the supplementary information (ESI, S3). All CV data are displayed following the IUPAC convention and the lower vertex voltage was 0.1 V in all cases. If not stated otherwise, the upper vertex potential was set to 2.0 V. During the anodic trace, the scan was held for 30 s at 0.7 V. For the determination of the PtO_x reduction charge, a polynomial base line of degree 5 was fitted the curves between 0.5 V and 1.2 V. The integration of the peak yielded the PtO_x reduction charge.

2.3 Kramers-Kronig validity test

The analysis of impedance data requires high quality data. The data must be a representation of a linear, time-invariant and causal system. The Kramers-Kronig relation is an approach to determine the validity of a spectrum a-posteriori.[55] They relate the real part of the impedance to the imaginary part and vice versa if all system requirements are fulfilled. In this work a linear Kramers-Kronig test was used with a μ-criterion to avoid over- and under-fitting as proposed by Schönleber et al.[56] The validity of the spectrum is considered to be fulfilled when the residuals are smaller than 1% and no bias can be observed over the whole frequency range. The fitting model required for the linear Kramers-Kronig test consisted of an ohmic resistance and inductor and a variable number of R/C elements in series. All impedance spectra shown in this work are valid according to the Kramers-Kronig relation. The respective residuals for the used frequency range of 10 kHz to 100 mHz are given in the supplementary information (ESI, S4).

3 Results and discussion

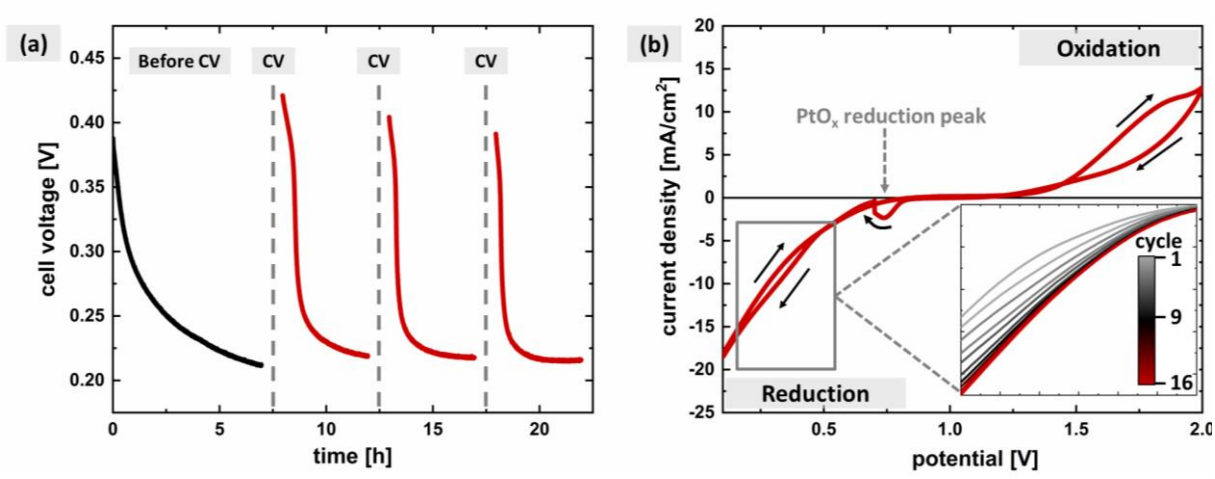

Figure 1 (a) Constant current measurement (10 mA cm^{-2}) of a CP/Pt@CDP MEA, intermitted by cyclic voltammetry (CV) measurements, marked as grey dashed lines. After each CV measurement the voltage increased to the initial level of the measurement before decreasing again. After the first CV, a change in the degradation speed occurred. (b) Representative cycle from the CV measurement consisting of 16 cycles between 0.1 V to 2.0 V conducted in (a). At 0.7 V the voltage remained constant for 30 s to ensure complete reduction of generated PtO_x. The inset shows the polarization curve between 0.2 V and 0.6 V depending on the cycle. The enhancement between each cycle is decreasing with the performance approaching a stable value after 16 cycles.

Electrodes with a thin catalyst layer have a very high platinum utilizations and enable the investigation of degradation mechanisms on a reasonable time scale.[11,48] Figure 1 (a) shows a representative voltage of a CP/Pt@CDP MEA at a constant current density of 10 mA cm^{-2} interrupted by CV measurements, as indicated by the grey dashed lines. Within the first 7 h, the cell voltage shows an fast asymptotic decrease from 0.4 V to 0.2 V. A similar trend was reported before for similar electrodes and conditions.[11] High performance SAFC electrodes are based on porous electrodes with well dispersed platinum and achieve both higher power densities and stability.[10,49] The presented electrode design however features a well observable but low area where platinum and CsH_2PO_4 are in contact. Large amounts of platinum were shown to be inactive with most of the reaction taking place in close proximity to the carbon fibers.[11] In a computational model Bertei et al.[57] showed that inhomogeneous

current distributions and the corresponding Joule heating in fuel cells are significantly underestimated by continuum approximations. Taking this into account, the current per mg of platinum is significantly higher in the presented electrodes compared to high performance electrodes and hotspots are more likely to occur.

In the following CV measurement, the cell voltage was cycled 16 times between 0.1 V and 2 V, Figure 1 (b). During this measurement, the platinum catalyst on the cathode side of the fuel cell is repeatedly oxidized and reduced. During the cathodic trace, higher oxides such as PtO_2 can be generated through oxygen vacancy diffusion depending on the voltage.[58,59] The onset and intensity of the PtO_x reduction during cycling is dependent on the upper vertex voltage and starts at around 0.9 V.[45,60,61] During the anodic trace, the CV measurement was held at a voltage of 0.7 V for 30 seconds to ensure a complete reduction of the generated PtO_x. Integration of the platinum reduction peak provides the amount of electrochemically accessible PtO_x. Liu et al reported the reversibility of the PtO_x formation.[62] After the CV measurement, the cell voltage increased to over 0.4 V during CC, representing a significant increase in the power output. During the further course of the CC measurement, an asymptotic decrease to 0.2 V occurred again but in a shorter period compared to the initial decrease. Further CV measurement resulted in a reproducible performance increase followed by an asymptotic decrease. Multiple cells were investigated and showed the same behavior (ESI, S5). The observed decrease of the maximum voltage after each CV measurement however did not occur in all samples and might not be significant. The inset in Figure **1** (b) shows the section of the polarization plot between 0.2 V and 0.6 V for select cycles of the CV measurement. The current density for each voltage is asymptotically increasing with each cycle. This enhancement effect is strongest after the first cycle, but multiple oxidation and reduction cycles are necessary to approach a stable performance. Variations in scan rate generally showed the same asymptotic increase. Both scan rate and oxidation time appear to have a positive effect on the increase in activity (ESI, S3).

The observed behavior indicates a degradation reaction which can be reversed by CV measurements. The change in the maximum voltage after each CV measurement can be caused by irreversible changes

like reduction of the active site density through changes of the electrode surface or microcrack formation, but further investigation is necessary.[11] The existence of different degradation mechanism for SAFC electrodes was already suggested by Lohmann-Richters.[46] Although the degradation is too fast to exploit this phenomenon for application, it provides valuable information about the degradation mechanism, enabling understanding and possibly prevention. For HT-PEMFC, a phosphate adsorption to the platinum catalyst on the cathode during operation is well known. During the electrochemical measurements in Figure 1, the cell voltage varied between 0.4 V and 0.2 V. At this voltage range the absorption of phosphate species (mainly $H_2PO_4^-$) at the surface of the cathodic catalyst had been reported for HT-PEMFC.[24] Subsequent, a reduction occurs generating strongly adsorbed phosphorous species which can poison the catalyst.[26,40–42] As reported previously, CsH_2PO_4 can undergo a morphological change during operating condition.[11] During this process the solid state of the electrolyte is lost and CsH_2PO_4 covers the platinum surface as seen in Figure 2, allowing an interaction between the $H_2PO_4^-$ groups and the catalyst. This process is most pronounced close to the current collector fibers and can lead to a higher number of triple phase boundaries. However previous studies have shown that the activity is decreasing with the increase of these surface changes and the observed reactivation cannot be attributed to the change in the triple phase boundaries.[11] The labeling of the phases was verified by energy-dispersive X-ray spectroscopy and back-scattered electron imaging (ESI, S1). Based on the observed morphological changes, different degradation mechanism were discussed in literature.[10,11,18] By covering the platinum surface, CsH_2PO_4 blocks the access of the gas phase, reducing the active area of the electrode. Since the changes in morphology are greatest near the current collectors, deterioration of the electrical contact between the current collector and the platinum surface can also lead to a reduction in activity. However, these degradation mechanisms cause irreversible damage and cannot be reversed by a CV measurement. The reproducible increase in activity to nearly the initial value strongly suggests that a reversible degradation process dominates. It should be noted that the measured performance enhancement represents truly faradaic currents. The CV measurement end on a back cycle, resulting in a complete reduction of all generated PtO_x. Also,

the total surplus charge after reactivation until stabilization is orders of magnitude higher than any possible surface capacitance could account for.

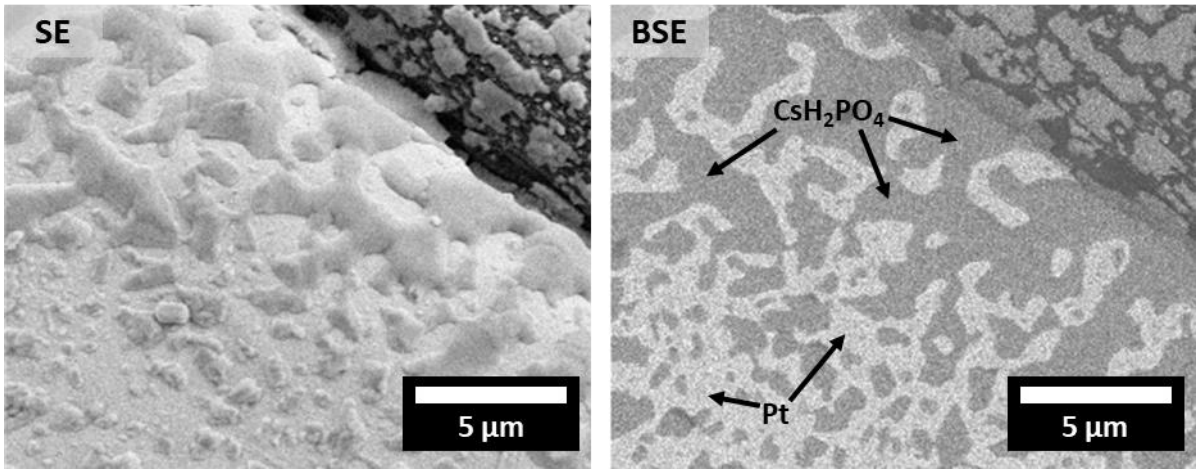

Figure 2 SEM micrographs of the cathode surface after 15 h of operation at a constant current of 10 mA cm^{-2}. The initially homogenous platinum layer is penetrated by CsH_2PO_4 which is partly covering the platinum surface. On the left, the surface topography was recorded with a secondary electron detector (SE). On the right, the same section was imaged with a backscattered electron detector (BSE) and the phases labelled based on the material-dependent electron backscattering intensity.

The overpotential of the ORR is much larger than the HOR and a potential phosphate poisoning of the anode is not influencing the cell performance significantly for HT-PEMFC.[35] It will be shown later that the same is true for SAFC. The speed of the degradation differs between before and after the first CV measurement, Figure 1 (a). After the first CV measurement, the decline of the voltage over time was highly reproducible. During the cathodic trace of the CV measurement, the platinum surface as well as phosphorus species present at the cathode surface are oxidized. The repeated oxidization and reduction of the catalyst surface at 240 °C may lead to a cleaning of the platinum surface by freeing previously blocked catalytic sites, ultimately reactivating the cell to its initial performance. However, during the following constant current measurement, the same poisoning is reoccurring. The cause of the difference between the degradation before and after the first CV measurement is unclear. Based on our work, two scenarios are conceivable: (1) The CV measurements are forcing all phosphorous

adsorbates out of the active centers, but because CsH_2PO_4 penetrated and spread across the platinum surface as shown in Figure 2, a faster poisoning can occur in the subsequent CC measurement. (2) After oxidation, the mobile phosphate anions remain adsorbed to the catalyst but do not significantly interfere with the ORR until reduced. Work of Prokop et al. done at 160 °C with concentrated phosphoric acid shows low cathodic currents at a potential of 0.43 V vs. DHE caused by the reduction of phosphate anions. These currents decrease over the course of hours indicating a rather slow reaction kinetic.[26] It is therefore reasonable to assume that the reduction of the phosphate anions in our cells at 240 °C happen with a similar speed, which is matching the observed degradation time scale.

Nyquist plots for representative SPEIS Measurements of a CP/Pt@CDP MEA without reactivation are shown in Figure 3 for voltages of 0.05 V and 0.35 V with a frequency range of 10 kHz to 100 mHz. The electrolyte resistance obtained from the high frequency x-axis intersection remained stable while the charge transfer resistance of the electrodes increased during the measurement, which agrees with the observed decline in performance. The depressed symmetry of the Nyquist semicircle is the result of a distributed time constant and was discussed previously, with the change in the surface morphology over time and other reactive processes suggested as cause.[11,63] Additional to the ohmic and capacitive resistance, the impedance spectra show incomplete inductive loops for frequencies <1 Hz. This low frequency inductive behavior is common for fuel cells and can be caused by variety of process effects e.g. reaction intermediates, side reaction, platinum oxidation and dissolution.[63–65] Schiefer et al. recently reported for LT-PEMFC, that reactions related to the ORR are dominating the low frequency inductive response, but multiple mechanisms are responsible to completely explain the observed effect.[66] All presented data in the frequency range from 10 kHz to 100 mHz is consistent with the Kramers-Kronig relation, hence the low frequency inductive loops are not caused by non-stationary effects during the impedance measurement. The inductive loop is voltage dependent and increases with time, being most distinct for a voltage of 0.05 V, while only small incomplete loops can be seen for U = 0.35 V, Figure 3 (a). Measuring impedance spectra close to DC conditions is not feasible due to the very long required measurement times. However, the slope of the I-V characterization curve gives

a good estimate for the nominal zero-frequency impedance. Figure 3 (b) shows selected Nyquist plots with arrows indicating the respective resistance obtained from the slope of the I-V characterization curve. While a much larger inductive loop could have been obtained at lower frequencies for Nyquist plots at 0.05 V, only a small difference is observed for 0.35 V. The process responsible for the inductive loop is therefore more pronounced for low voltages. The observed voltage and time dependency of the low frequency domain in Figure 3 indicates a slow poisoning side reaction which is most pronounced for low voltages. In the light of the discussed literature for HT-PEMFCs, a slow reduction of adsorbed phosphate ions seems likely as the cause. However, platinum oxide formation can generate a similar inductive behavior without the severe poisoning. Both processes are most likely happening simultaneously and cannot be differentiated by impedance spectroscopy alone.

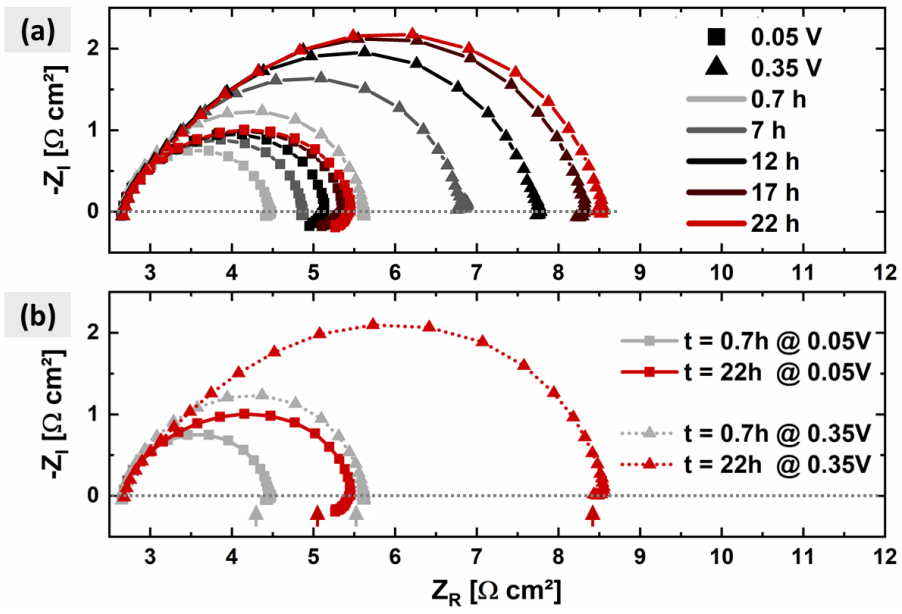

Figure 3 Impedance measurements of a CP/Pt@CDP MEA at different times and voltages relative to the pseudo-reference electrode. The arrows indicate the nominal zero-frequency impedance obtained from the IVC curves. Spectra are shown for a frequency range of 10 kHz to 100 mHz.

For HT-PEMFC phosphate adsorption of the anode side occurs but increases the overpotential of the HOR negligibly compared to the much larger overpotential of the ORR.[35] In Figure 4, two asymmetric Pt/CDP/powder MEAs with a rate limiting Pt thin film electrode on one side and a high performance

powder electrode on the other side were analyzed during a constant voltage measurement. In Figure **4** (lower part) the reaction was limited by the platinum thin film electrode of the cathode side. Changes in the overall performance are caused only by changes of the cathode. CV measurements to reactivate the catalyst were conducted every four hours, interrupting the CC measurements. With increasing degradation of the cell, the reactivation increased as well, showing that the CV measurements are reversing an effect happening to the cathode during degradation. When on the other hand the placement of the electrodes is switched and the rate limiting platinum thin film electrode is placed as the anode, the overall cell performance increased due to the increased cathode surface, Figure 4 (upper part). After the CV measurements, an initial deactivation instead of a reactivation is observed. The HOR at the anode is generally faster compared to the ORR at the cathode. Changing the anode in the MEA presented in Figure 4 (upper part) from the platinum thin film anode to a high-performance powder electrode resulted in a significant increase in activity (ESI, S6), indicating a rate limitation of the anode. During CV measurements carbon corrosion at the cathode side could cause severe degradation to a point where it affects the overall cell performance. The harsh conditions and high current densities during CV may also affect the anode and lead to a loss of activity, e.g., due to changes in the CsH_2PO_4 morphology and isolation of the current collectors as described previously, which do not occur at the anode during CC measurements.[11] At this point, further fundamental studies are required to fully understand the mechanism responsible for the observed deactivation. The absence of the reactivation in Figure 4 (upper part) however confines the phosphate poisoning to the cathode side, as reported for HT-PEMFC.[35]

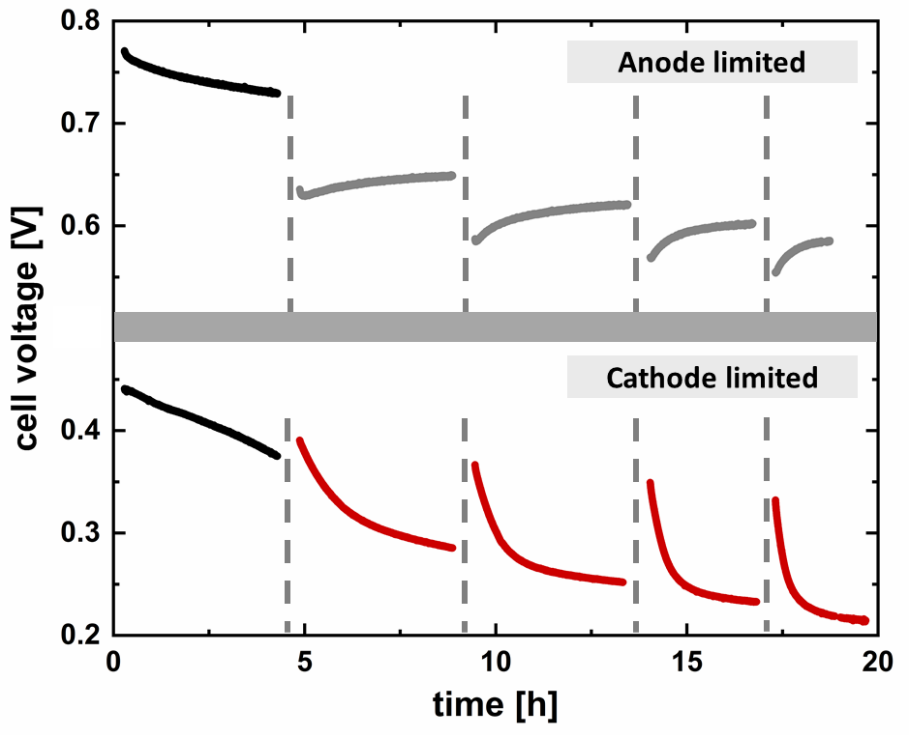

Figure 4 CC measurement (10 mA cm^{-2}) of two different, asymmetrical Pt/CDP/powder MEAs each consisting of a rate determining Pt thin film electrode and a state of the art powder electrode. Lower part: The rate determining Pt thin film electrode act as cathode. A decrease of the cell voltage is observed over time, intermitted by the activation after each CV. The intensity of the activation is increasing with proceeding degradation over time. Upper part: The rate determining Pt thin film electrode act as anode. The initial voltage is above 0.75 V since the performance of the cathode is increase. While the voltage during the CC measurement is relatively stable, after each CV measurement a decrease instead of an increase is observed.

The voltage of CP/Pt@CDP MEAs was measured at a constant current density of 10 mA cm^{-2} interrupted by CV measurements with varying upper vertex voltages. The value of the vertex voltage for each CV measurement taking place prior to the constant current measurement is given in Figure **5** (a). The current density at a representative voltage of 0.2 V of every second cycle during each CV measurements and the corresponding charge of the PtO_x reduction peak are shown vs the upper vertex voltage in Figure 5 (b). The current density at 0.2 V was chosen to quantify the activity increase of the cell during the CV measurement. After an initial stabilization time (Figure 5 (a); black), a CV

measurement with a vertex voltage of 2.0 V lead to the already observed reactivation, even though the cell performance did not stabilize. The intensity of the reactivation decreased with decreasing upper vertex voltage until no further activation was observed below 1.7 V. By comparing Figure 5 (a) and (b) a correlation between the reactivation intensity, the current density and the charge of the PtO_x reduction peak is evident. The measured current density at 0.2 V as well as the charge of the PtO_x reduction peak increase significantly with the cycle number for an upper vertex voltage 1.8 V and higher, with the highest increase at 2.0 V. For these vertex voltages, a significant reactivation after CV measurements occurred. No increase of the current density or the PtO_x reduction charge on the other hand was detected for upper vertex potentials of 1.7 V and lower, for which a decrease of the cell voltage instead of an increase after CV measurements was observed. This could be an effect generally caused by the fast, repetitive cycling but concealed by the activity increase for higher vertex voltages. These results show a connection between the increase of the PtOx reduction charge during CV and the strength of the reactivation after the CV measurement.

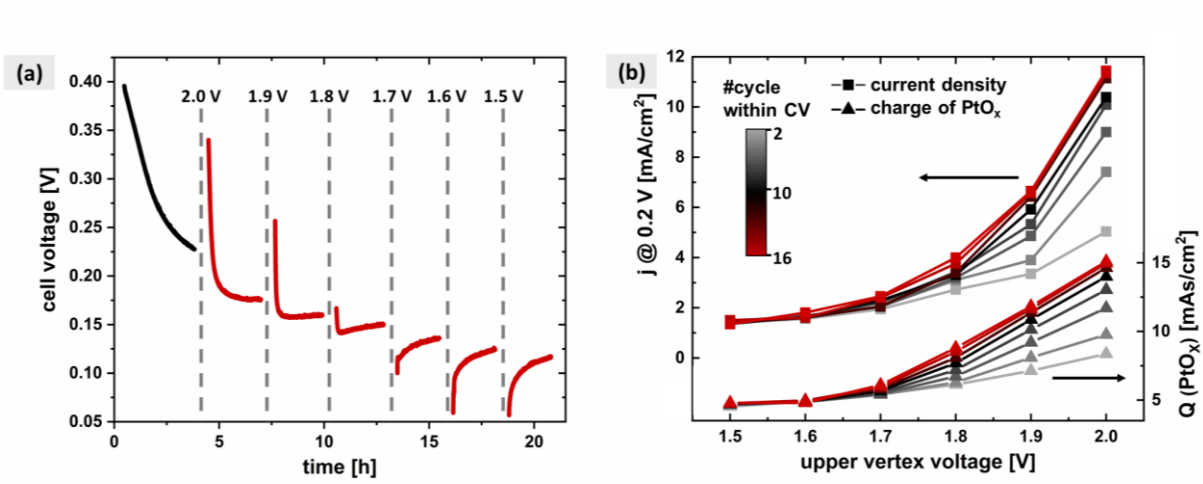

Figure 5 (a) constant current measurements (10 mA cm^{-2}) intermitted by CV measurements with different upper vertex voltages. (b) Is a closer investigation of the respective CV measurements conducted in (a). Shown is the current density at a representative voltage of 0.2 V (left axis) and the charge calculated from the PtO_x reduction peak (right axis) vs the upper vertex voltages for every other cycle during the CV measurements.

In-operando spectroscopy to detect the formation and reaction of adsorbed compounds is very challenging and requires special techniques and modified experimental set up, which are currently not available. Thus, we can only assume that the previous findings concerning HT-PEMFCs can be transferred to SAFC electrodes. In operando μ-XANES characterization by Kaserer et al. showed a phosphate adsorption on the platinum during fuel cell operation for a voltage range between 300 mV and 800 mV vs. a reversible hydrogen electrode.[24] Above a voltage of 800 mV, the increasing adsorption of oxygen species forces a change of the phosphate adsorption geometry from double coordinated C_{2V} geometry to the single coordinated C_S symmetry.[29] In operando μ-XANES as applied by Kaserer et al. cannot detect this adsorption geometry due to its high mobility. They reported that phosphate even at high voltages may not leave the surface.[24] As mentioned before, phosphate species are reduced after adsorption during electrochemical measurements. At 300 mV and below, hydrogen originating from the ORR and the electrolyte is present even at the cathode side, facilitating a reduction to H_3PO_3, H_3PO_2 and even elemental phosphorous.[26,40–42] The oxidation of such phosphorous species, which tend to adsorb strongly on the catalyst, requires high voltages and is accompanied by platinum oxidation.[41,42]These processes correlate well with our findings. As seen in Figure 5 (b) the formation of larger quantities of platinum oxide is accompanied with a successful reactivation of the cell. A widely accepted mechanism of the platinum oxidation is based on a platinum atom extraction from the bulk into the oxidation adsorbate layer once a sufficient loading is reached.[58] Hence, an equivalent of two PtO layers is generated for each monolayer of adsorbed oxygen. Via oxygen vacancy diffusion at increased voltages, higher oxides such as PtO_2 can be generated as well.[58] Studies at room temperature showed a generation of amorphous 3D α-PtO_2 for voltages above 1.3 V.[59] During the process of the platinum atom diffusion and oxide layer formation, phosphorous adsorbates may get forced out from the active sites. Variations in CV scan speed showed that multiple oxidation and reduction cycles as well as longer oxidation times are beneficial for the reactivation (ESI, S3). It is also possible that phosphorous species are oxidized at high voltages while the generated phosphate anions are still

adsorbed at the surface. Due to the C_s coordination symmetry and the high mobility, these anions are blocking the ORR much less than the reduced ones. When cells where operated at voltages above the reduction conditions for phosphate anions, enhanced stability is observed.[11] At this voltage regions, either PO_4^{3-} is not reduced or the current density is insufficient to cause a morphological change and CsH_2PO_4 stays in its solid form, preventing a platinum poisoning.

Ex-situ XPS measurements after electrochemical characterization under 10 mA cm^{-2} for 15 h showed an increased intensity of the P2p peak compared to an as-fabricated cell without electrochemical characterization. The intensity increase can be attributed to the electrolyte creep discussed in Figure **2** as well as micro crack formation and surface damage during measurement.[11] A shift to higher binding energies can be seen, most pronounced for the cathode. A change in the binding energy is the result of different phosphorous environments and can indicate a change in the oxidation state caused, for example, by phosphate reduction during fuel cell operation.[67] After separation of the platinum layer from the electrolyte by multiple washing steps, a small difference in the intensity and no shift of the binding energy occurred between the cathode and as-fabricated catalyst layer (ESI, S7). Analyzation of the Pt4f region did not indicate any change in the platinum oxidation state. The information value of ex-situ measurements for this problem must be considered carefully, since reduced species might not be stable.

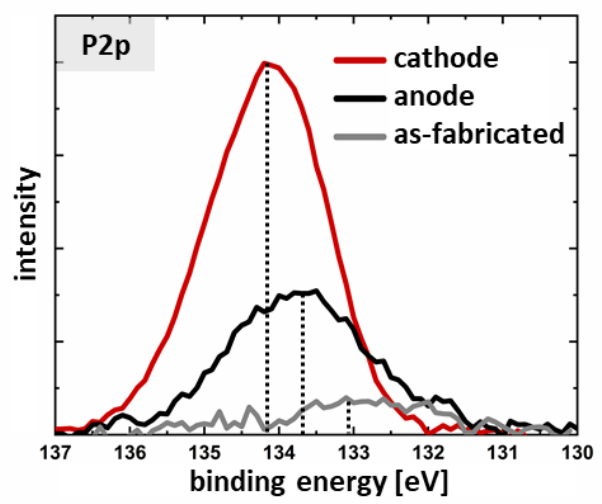

Figure 6 X-ray photoelectron spectroscopy analysis in the P2p region for the cathode (red), anode (black) and as-fabricated electrode (grey), collected from platinum thin layer (60 nm) on CsH_2PO_4. Except for the as-fabricated MEA, cells operated for 15 h at a constant current of 10 mA cm^{-2}.

The presented measurements in total strongly indicate a phosphorous associated poisoning of SAFCs during operation. This is in good agreement the work of Ghoshal et al., who showed a better stability of SAFC electrodes when utilizing phosphate tolerant catalysts.[20] Different strategies can be used to decrease or even prevent this process: Hatahet el al. showed promising results using graphene as a protective layer between CsH_2PO_4 and the catalyst to prevent the formation of phosphorous adsorbates. [publication is still under revision] Another approach is based on reducing local hot spots and related morphological changes of CsH_2PO_4, which would generate free $H_2PO_4^-$ species. A current collector with a micro porous layer enables a more uniform contact between the current collector and the catalyst layer, resulting in fewer hotspots and an improved stability.[11] A Pt@CP_{MPL}/CDP MEA utilizing such a micro porous layer was measured over 80 h at a constant current of 45 mA cm^{-2}, which was chosen to achieve a similar initial cell voltage as in Figure 1. With <125 µV h^{-1} the MEA showed a remarkable improvement of the stability (ESI, S8), especially compared to the rapid degradation of the CP/Pt@CDP MEA shown in Figure 1. Corresponding Nyquist plots of the Pt@CP_{MPL}/CDP MEA during the CC measurement are shown in Figure 7.

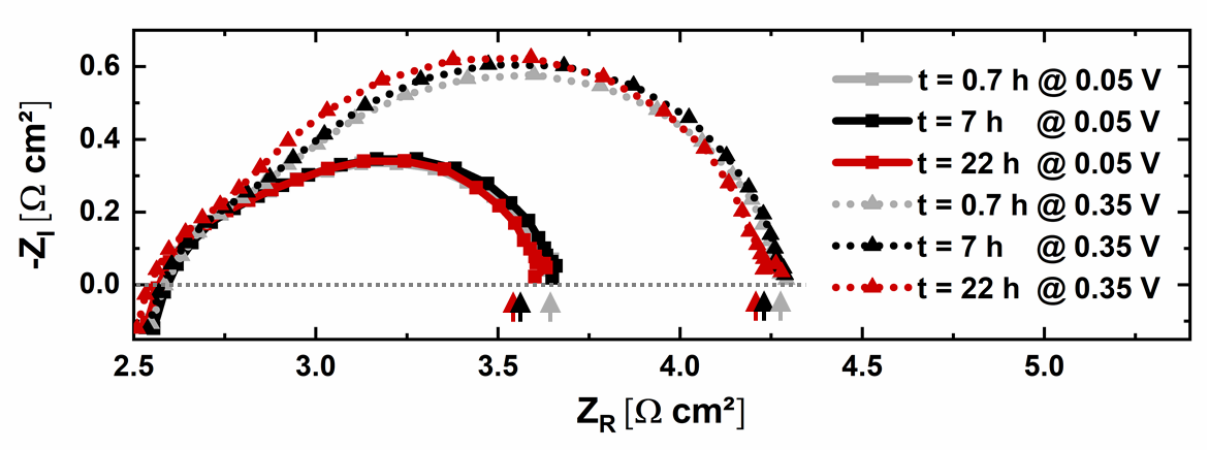

Figure 7 Impedance measurements of a Pt@CP_{MPL}/CDP MEA after different times and voltages relative to the pseudo-reference electrode. The arrows indicate the nominal zero-frequency impedance obtained from the IVC curves at the respective voltage. Spectra are shown for a frequency range of 10 kHz to 100 mHz.

Impedance spectra were recorded for voltages of 0.05 V and 0.35 V with a frequency range of 10 kHz to 100 mHz. Both the electrolyte resistance and the charge transfer resistance, associated with the ORR, remain stable within the time of the measurement. A similar depression of the semi-circle symmetry as in Figure 3 can be observed. However, no inductive loops are visible within the measured frequency range. Estimation of the nominal zero-frequency impedance, marked by the arrows in the respective color, shows no deviation after 0.7 h (red) and only small deviation after 7 h (black) and 22 h (green) for both 0.05 V and 0.35 V. The observed inductive loops can be caused by side reactions in general and the impedance measurements do not provide information about the involved species.[64] Based on our system, the formation of PtO_x and subsequent platinum dissolution as well as phosphate adsorption and reduction are the most likely side reactions. [24–26,64] Platinum oxidation at 160 °C begins at around 1 V vs. DHE after the surface has been gradually covered by electrosorbed oxygen atoms.[25] Lower onsets for platinum oxidations have been reported for LT-PEMFCs at 40 °C.[64] In any case, the voltage range of 0.4 v to 0.2 V, at which the cell degradation of study took place, is below well below oxidation onset voltage. This makes an oxide formation an unlikely cause for the observed inductive loops. Phosphate adsorption and reduction on the other hand have been reported for the voltages

below 0.4 V.[24,26] The phosphorous poisoning, which we therefore associate with the inductive loops, could be significantly reduced by the modification of the current collector. This is in good correlation with the high stability of the Pt@CP_{MPL}/CDP MEA, even though the measurement time scale is insufficient to exclude very slow poisoning processes. The improved stability can be the result of a decreased rate in the morphological change of the CsH_2PO_4 due to the more uniform electrical connection. While CsH_2PO_4 remains stable, the adsorption and reduction of phosphate anions is not or only very slowly occurring.

4 Conclusion

In this study, the degradation of solid acid fuel cell electrodes with a non-uniform current distribution was linked to a phosphorous poisoning of the platinum catalyst, well known from HT-PEMFC. By cycling MEAs between 0.1 V and 2.0 V for 16 times, the platinum catalyst was alternately oxidized and reduced. During these CV measurements, the activity increased asymptotically with the number of cycles. Afterwards, the activity of the cell increased significantly during constant current characterization reaching almost the initial value, followed again by a fast degradation. This process of activation and degradation triggered by CV measurements was highly reproducible and the cathode was identified as the origin of this effect and a dependency of the upper vertex voltage during the CV measurements is shown. The amount of PtO_x generated and reduced during the cycling is in good correlation with the increasing activity. It was proposed that the generation of PtO_x is accompanied by the oxidation of phosphorous species, generated during operation. The resulting phosphate adsorbate tends to block the ORR less than the reduced counterpart. A potential phosphate adsorption was supported by impedance measurements at different voltages. The observed voltage and time dependency of the low frequency domain may indicate a catalyst poisoning due to the slow reduction of adsorbed phosphate ions, which is most pronounced for low voltages. The presented results show that the morphological changes of the electrolyte play a central role in the performance degradation. Using a micro porous electron collector has shown reduced inductive loops in the impedance response and achieve a very high stability (<125 $\mu V\ h^{-1}$ at 0.43 V), most likely by preventing morphological changes

of the CsH_2PO_4 at the electrolyte/electrode boundary. While CsH_2PO_4 is morphologically stable, no catalyst poisoning is observed.

In summary, catalyst poisoning processes associated with the phosphate adsorption are still very relevant for solid acid fuel cells with the solid-state electrolyte CsH_2PO_4 as in HT-PEMFC where phosphoric acid is employed. Major improvements can be achieved with a suitable electrode design. Based on the presented results we propose the existence of liquid electrolyte due to local hotspots as root cause in the catalyst poisoning. This shows the importance of a solid acid electrolyte for intermediate fuel cells, as such can prevent the poisoning inherent to other intermediate fuel cells using phosphoric acid as electrolyte. The better understanding of the platinum degradation mechanism represents a step towards long term stable high-performance electrodes.

Conflicts of interest

There are no conflicts to declare.

Acknowledgements

The authors thank Petra Hertel for sputter deposition. Financial support of this work by the German Federal Environmental Organization (DBU), European Social Fund (ESF) and the Volkswagen Foundation is gratefully acknowledged.

References

1 R. E. Rosli, A. B. Sulong, W. Daud, M. A. Zulkifley, T. Husaini, M. I. Rosli, E. H. Majlan and M. A. Haque, A review of high-temperature proton exchange membrane fuel cell (HT-PEMFC) system, *International Journal of Hydrogen Energy*, 2017, **42**, 9293–9314.

2 S. M. Haile, H. Liu and R. A. Secco, High-Temperature Behavior of CsH 2 PO 4 under Both Ambient and High Pressure Conditions, *Chem. Mater.*, 2003, **15**, 727–736.

3 D. A. Boysen, T. Uda, C. R. I. Chisholm and S. M. Haile, High-performance solid Acid fuel cells through humidity stabilization, *Science (New York, N.Y.)*, 2004, **303**, 68–70.

4 A. Goñi-Urtiaga, D. Presvytes and K. Scott, Solid acids as electrolyte materials for proton exchange membrane (PEM) electrolysis: Review, *International Journal of Hydrogen Energy*, 2012, **37**, 3358–3372.
5 O. Paschos, J. Kunze, U. Stimming and F. Maglia, A review on phosphate based, solid state, protonic conductors for intermediate temperature fuel cells, *Journal of physics. Condensed matter : an Institute of Physics journal*, 2011, **23**, 234110.
6 A. I. Baranov, V. P. Khiznichenko, V. A. Sandler and L. A. Shuvalov, Frequency dielectric dispersion in the ferroelectric and superionic phases of CsH 2 PO 4, *Ferroelectrics*, 1988, **81**, 183–186.
7 J. Otomo, Protonic conduction of CsH2PO4 and its composite with silica in dry and humid atmospheres, *Solid State Ionics*, 2003, **156**, 357–369.
8 Y. Taninouchi, T. Uda, Y. Awakura, A. Ikeda and S. M. Haile, Dehydration behavior of the superprotonic conductor CsH2PO4 at moderate temperatures: 230 to 260 °C, *J. Mater. Chem.*, 2007, **17**, 3182.
9 Y. Taninouchi, T. Uda and Y. Awakura, Dehydration of CsH2PO4 at temperatures higher than 260 °C and the ionic conductivity of liquid product, *Solid State Ionics*, 2008, **178**, 1648–1653.
10 A. B. Papandrew, R. A. Elgammal, M. Tian, W. D. Tennyson, C. M. Rouleau, A. A. Puretzky, G. M. Veith, D. B. Geohegan and T. A. Zawodzinski, Nanostructured carbon electrocatalyst supports for intermediate-temperature fuel cells: Single-walled versus multi-walled structures, *Journal of Power Sources*, 2017, **337**, 145–151.
11 M. Wagner, O. Lorenz, F. P. Lohmann-Richters, A. Varga and B. Abel, On the role of local heating in cathode degradation during the oxygen reduction reaction in solid acid fuel cells, *Sustainable Energy Fuels*, 2020, **4**, 5284–5293.
12 Q. Li, R. He, J. O. Jensen and N. J. Bjerrum, PBI-Based Polymer Membranes for High Temperature Fuel Cells– Preparation, Characterization and Fuel Cell Demonstration, *Fuel Cells*, 2004, **4**, 147–159.
13 F. P. Lohmann, P. S. C. Schulze, M. Wagner, O. Naumov, A. Lotnyk, B. Abel and Á. Varga, The next generation solid acid fuel cell electrodes: stable, high performance with minimized catalyst loading, *J. Mater. Chem. A*, 2017, **5**, 15021–15025.
14 A. B. Papandrew, S. St. John, R. A. Elgammal, D. L. Wilson, R. W. Atkinson, J. S. Lawton, T. M. Arruda and T. A. Zawodzinski, Vapor-Deposited Pt and Pd-Pt Catalysts for Solid Acid Fuel Cells: Short Range Structure and

Interactions with the CsH 2 PO 4 Electrolyte, *J. Electrochem. Soc.*, 2016, **163**, F464-F469.
15 Y. Xiao and L. Tang, High-Throughput Approach Exploitation: Two-Dimensional Double-Metal Sulfide (M 2 S 2) of Efficient Electrocatalysts for Oxygen Reduction Reaction in Fuel Cells, *Energy Fuels*, 2020, **34**, 5006–5015.
16 A. B. Papandrew, C. R. I. Chisholm, R. A. Elgammal, M. M. Özer and S. K. Zecevic, Advanced Electrodes for Solid Acid Fuel Cells by Platinum Deposition on CsH 2 PO 4, *Chem. Mater.*, 2011, **23**, 1659–1667.
17 A. COLLIER, H. WANG, X. ZIYUAN, J. ZHANG and D. WILKINSON, Degradation of polymer electrolyte membranes, *International Journal of Hydrogen Energy*, 2006, **31**, 1838–1854.
18 C. R. I. Chisholm, D. A. Boysen, A. B. Papandrew, S. Zecevic, S. Cha, K. A. Sasaki, Á. Varga, K. P. Giapis and S. M. Haile, From Laboratory Breakthrough to Technological Realization: The Development Path for Solid Acid Fuel Cells, *The Electrochemical Society Interface*, 2009, 53–59.
19 V. S. Thoi, R. E. Usiskin and S. M. Haile, Platinum-decorated carbon nanotubes for hydrogen oxidation and proton reduction in solid acid electrochemical cells, *Chem. Sci.*, 2015, **6**, 1570–1577.
20 S. Ghoshal, Q. Jia, J. Li, F. Campos, C. R. Chisholm and S. Mukerjee, Electrochemical and In Situ Spectroscopic Evidences toward Empowering Ruthenium-Based Chalcogenides as Solid Acid Fuel Cell Cathodes, *ACS Catal.*, 2017, **7**, 581–591.
21 R. Zeis, Materials and characterization techniques for high-temperature polymer electrolyte membrane fuel cells, *Beilstein Journal of Nanotechnology*, 2015, **6**, 68–83.
22 M. Prokop, M. Drakselova and K. Bouzek, Review of the experimental study and prediction of Pt-based catalyst degradation during PEM fuel cell operation, *Current Opinion in Electrochemistry*, 2020, **20**, 20–27.
23 P. Bindra, Platinum Dissolution in Concentrated Phosphoric Acid, *J. Electrochem. Soc.*, 1979, **126**, 1631.
24 S. Kaserer, K. M. Caldwell, D. E. Ramaker and C. Roth, Analyzing the Influence of H 3 PO 4 as Catalyst Poison in High Temperature PEM Fuel Cells Using in-operando X-ray Absorption Spectroscopy, *Journal of Physical Chemistry C*, 2013, **117**, 6210–6217.
25 M. Prokop, R. Kodym, T. Bystron, M. Paidar and K. Bouzek, Degradation kinetics of Pt during high-temperature PEM fuel cell operation part I:

Kinetics of Pt surface oxidation and dissolution in concentrated H3PO4 electrolyte at elevated temperatures, *Electrochimica Acta*, 2019, **313**, 352–366.
26 M. Prokop, R. Kodym, T. Bystron, M. Drakselova, M. Paidar and K. Bouzek, Degradation kinetics of Pt during high-temperature PEM fuel cell operation part II: Dissolution kinetics of Pt incorporated in a catalyst layer of a gas-diffusion electrode, *Electrochimica Acta*, 2020, **333**, 135509.
27 S. Ye, H. Kita and A. Aramata, Hydrogen and anion adsorption at platinum single crystal electrodes in phosphate solutions over a wide range of pH, *Journal of Electroanalytical Chemistry*, 1992, **333**, 299–312.
28 S. S. Araya, F. Zhou, V. Liso, S. L. Sahlin, J. R. Vang, S. Thomas, X. Gao, C. Jeppesen and S. K. Kaer, A comprehensive review of PBI-based high temperature PEM fuel cells, *International Journal of Hydrogen Energy*, 2016, **41**, 21310–21344.
29 F. C. Nart and T. Iwasita, On the adsorption of H2PO−4 and H3PO4 on platinum: an in situ FT-ir study, *Electrochimica Acta*, 1992, **37**, 385–391.
30 Q. He, B. Shyam, M. Nishijima, D. Ramaker and S. Mukerjee, Mitigating Phosphate Anion Poisoning of Cathodic Pt/C Catalysts in Phosphoric Acid Fuel Cells, *Journal of Physical Chemistry C*, 2013, **117**, 4877–4887.
31 Q. He, X. Yang, W. Chen, S. Mukerjee, B. Koel and S. Chen, Influence of phosphate anion adsorption on the kinetics of oxygen electroreduction on low index Pt(hkl) single crystals, *Physical chemistry chemical physics : PCCP*, 2010, **12**, 12544–12555.
32 Z. Liu, J. S. Wainright, M. H. Litt and R. F. Savinell, Study of the oxygen reduction reaction (ORR) at Pt interfaced with phosphoric acid doped polybenzimidazole at elevated temperature and low relative humidity, *Electrochimica Acta*, 2006, **51**, 3914–3923.
33 P. Stonehart, Development of alloy electrocatalysts for phosphoric acid fuel cells (PAFC), *J Appl Electrochem*, 1992, **22**, 995–1001.
34 M. Benabdellah and B. Hammouti, Corrosion behaviour of steel in concentrated phosphoric acid solutions, *Applied Surface Science*, 2005, **252**, 1657–1661.
35 K. M. Caldwell, S. Kaserer, C. Roth and D. E. Ramaker, Following Adsorbate Coverage on Anodes of High-Temperature Polymer Electrolyte Membrane Fuel Cells in the Presence of CO and H2O by using

InOperando X-ray Absorption Spectroscopy, *Chemelectrochem*, 2015, **2**, 1502–1509.
36 M. Weber, F. C. Nart, I. R. de Moraes and T. Iwasita, Adsorption of Phosphate Species on Pt(111) and Pt(100) As Studied by in Situ FTIR Spectroscopy, *J. Phys. Chem.*, 1996, **100**, 19933–19938.
37 P. Zelenay, A Comparison of the Properties of CF[sub 3]SO[sub 3]H and H[sub 3]PO[sub 4] in Relation to Fuel Cells, *J. Electrochem. Soc.*, 1986, **133**, 2262.
38 N. Sugishima, Phosphorous Acid Impurities in Phosphoric Acid Fuel Cell Electrolytes: II Effects on the Oxygen Reduction Reaction at Platinum Electrodes, *J. Electrochem. Soc.*, 1994, **141**, 3332.
39 N. Sugishima, Phosphorous Acid Impurities in Phosphoric Acid Fuel Cell Electrolytes: I Voltammetric Study of Impurity Formation, *J. Electrochem. Soc.*, 1994, **141**, 3325.
40 W. H. Doh, L. Gregoratti, M. Amati, S. Zafeiratos, Y. T. Law, S. G. Neophytides, A. Orfanidi, M. Kiskinova and E. R. Savinova, Scanning Photoelectron Microscopy Study of the Pt/Phosphoric-Acid-Imbibed Membrane Interface under Polarization, *Chemelectrochem*, 2014, **1**, 180–186.
41 M. Prokop, T. Bystron and K. Bouzek, Electrochemistry of Phosphorous and Hypophosphorous Acid on a Pt electrode, *Electrochimica Acta*, 2015, **160**, 214–218.
42 M. Prokop, T. Bystron, M. Paidar and K. Bouzek, H3PO3 electrochemical behaviour on a bulk Pt electrode: adsorption and oxidation kinetics, *Electrochimica Acta*, 2016, **212**, 465–472.
43 W. M. Vogel and J. M. Baris, Changes in the surface of platinum in hot concentrated phosphoric acid at low potentials, *Electrochimica Acta*, 1978, **23**, 463–466.
44 S. J. Clouser, J. C. Huang and E. Yeager, Temperature dependence of the Tafel slope for oxygen reduction on platinum in concentrated phosphoric acid, *J Appl Electrochem*, 1993, **23**, 597–605.
45 F. P. Lohmann-Richters, B. Abel and Á. Varga, In situ determination of the electrochemically active platinum surface area: key to improvement of solid acid fuel cells, *J. Mater. Chem. A*, 2018, **6**, 2700–2707.
46 F. P. Lohmann-Richters, Universität Leipzig, 2018.
47 R. C. Suryaprakash, F. P. Lohmann, M. Wagner, B. Abel and A. Varga, Spray drying as a novel and scalable fabrication method for

nanostructured CsH 2 PO 4 Pt-thin-film composite electrodes for solid acid fuel cells, *Rsc Advances*, 2014, **4**, 60429–60436.
48 M. W. Louie and S. M. Haile, Platinum thin film anodes for solid acid fuel cells, *Energy Environ. Sci.*, 2011, **4**, 4230.
49 D.-K. Lim, J. Liu, S. A. Pandey, H. Paik, C. R. Chisholm, J. T. Hupp and S. M. Haile, Atomic layer deposition of Pt@CsH2PO4 for the cathodes of solid acid fuel cells, *Electrochimica Acta*, 2018, **288**, 12–19.
50 M. Wagner, C. Dreßler, F. P. Lohmann-Richters, K. Hanus, D. Sebastiani, A. Varga and B. Abel, Mechanism of ion conductivity through polymer-stabilized CsH 2 PO 4 nanoparticular layers from experiment and theory, *J. Mater. Chem. A*, 2019, **7**, 27367–27376.
51 T. Uda and S. M. Haile, Thin-Membrane Solid-Acid Fuel Cell, *Electrochem. Solid-State Lett.*, 2005, **8**, A245-A246.
52 J. A. Shetzline, S. Bukola and S. E. Creager, A convenient miniature test platform for polyelectrolyte membrane fuel-cell research, *Journal of Electroanalytical Chemistry*, 2017, **797**, 8–15.
53 S. Torija, L. Prieto-Sanchez and S. J. Ashton, In-situ electrochemically active surface area evaluation of an open-cathode polymer electrolyte membrane fuel cell stack, *Journal of Power Sources*, 2016, **327**, 543–547.
54 E. Brightman, G. Hinds and R. O'Malley, In situ measurement of active catalyst surface area in fuel cell stacks, *Journal of Power Sources*, 2013, **242**, 244–254.
55 B. A. Boukamp, A Linear Kronig‐Kramers Transform Test for Immittance Data Validation, *J. Electrochem. Soc.*, 1995, **142**, 1885–1894.
56 M. Schönleber, D. Klotz and E. Ivers-Tiffée, A Method for Improving the Robustness of linear Kramers-Kronig Validity Tests, *Electrochimica Acta*, 2014, **131**, 20–27.
57 A. Bertei, V. Yufit, F. Tariq and N. P. Brandon, A novel approach for the quantification of inhomogeneous 3D current distribution in fuel cell electrodes, *Journal of Power Sources*, 2018, **396**, 246–256.
58 H. A. Baroody, G. Jerkiewicz and M. H. Eikerling, Modelling oxide formation and growth on platinum, *The Journal of chemical physics*, 2017, **146**, 144102.
59 Y.-F. Huang, P. J. Kooyman and M. T. M. Koper, Intermediate stages of electrochemical oxidation of single-crystalline platinum revealed by in situ Raman spectroscopy, *Nature communications*, 2016, **7**, 12440.

60 T. SUZUKI and Y. MORIMOTO, Kinetics of Oxide Formation and Reduction at Pt Catalyst in Polymer Electrolyte Fuel Cells, *Electrochemistry*, 2016, **84**, 511–515.
61 A. N. Correia, L. H. Mascaro, S. Machado and L. A. Avaca, Active surface area determination of Pd-Si alloys by H-adsorption, *Electrochimica Acta*, 1997, **42**, 493–495.
62 Y. Liu, M. Mathias and J. Zhang, Measurement of Platinum Oxide Coverage in a Proton Exchange Membrane Fuel Cell, *Electrochem. Solid-State Lett.*, 2010, **13**, B1.
63 B. P. Setzler and T. F. Fuller, A Physics-Based Impedance Model of Proton Exchange Membrane Fuel Cells Exhibiting Low-Frequency Inductive Loops, *J. Electrochem. Soc.*, 2015, **162**, F519-F530.
64 S. K. Roy, M. E. Orazem and B. Tribollet, Interpretation of Low-Frequency Inductive Loops in PEM Fuel Cells, *J. Electrochem. Soc.*, 2007, **154**, B1378.
65 G. A. Futter, P. Gazdzicki, K. A. Friedrich, A. Latz and T. Jahnke, Physical modeling of polymer-electrolyte membrane fuel cells: Understanding water management and impedance spectra, *Journal of Power Sources*, 2018, **391**, 148–161.
66 A. Schiefer, M. Heinzmann and A. Weber, Inductive Low - Frequency Processes in PEMFC - Impedance Spectra, *Fuel Cells*, 2020, **20**, 499–506.
67 C. Powell, *X-ray Photoelectron Spectroscopy Database XPS,Version 4.1, NIST Standard Reference Database 20*, 1989.